Taylor & Francis
Taylor & Francis Group

Check for updates

Platinum-free counter electrodes of plasma-modified hybrid nanomaterials for dye-sensitised solar cells

Sule Erten-Ela[a], Melek Kiristi[b], Ana Varlec[c], Ferhat Bozduman[d], Maja Remskar[c], Lutfi Oksuz[d] and Aysegul Uygun Oksuz[b]

[a]Solar Energy Institute, Ege University, Izmir, Turkey; [b]Faculty of Arts and Science, Department of Chemistry, Suleyman Demirel University, Isparta, Turkey; [c]Solid State Physics Department, Jozef Stefan Institute, Ljubljana, Slovenia; [d]Faculty of Arts and Science, Department of Physics, Suleyman Demirel University, Isparta, Turkey

ABSTRACT

Molybdenum disulphide (MoS_2) nanotube and tungsten oxide ($W_{18}O_{49}$) nanowire were coated with poly(3-hexylthiophene) (P3HT) and poly(3,4-ethylenedioxythiophene) (PEDOT) by a radio frequency (RF: 13.56 MHz)-rotating plasma-modification method as alternative counter electrodes for dye-sensitised solar cells (DSSCs). Surface analysis showed the homogenous plasma nanocoating of inorganic nanostructures by P3HT and PEDOT. It was demonstrated that the plasma-modified hybrid platinum-free counter electrodes increased the efficiencies of the DSSCs. The DSSCs based on hybrid nanostructure materials showed a short circuit current density of 9.49, 7.95, 2.59 and 2.57 $mAcm^{-2}$ for MoS_2/P3HT, MoS_2/PEDOT, $W_{18}O_{49}$/PEDOT and $W_{18}O_{49}$/P3HT samples, respectively. The plasma nanocoating with the nanostructured materials approach for obtaining hybrid counter electrodes in the photovoltaic action shows an alternative route towards cost-effective, green energy conversion.

1. Introduction

Since 1991, dye-sensitised solar cells (DSSCs) have found academic and commercial attention around the world due to their low cost-effectiveness and simple fabrication (O'Regan and Grätzel 1991; Zhang et al. 2013; Susanti et al. 2014). The properties of working electrode (Huang, Pien, and Kuo 2014), counter electrode (Thomas et al. 2014; Briscoe and Dunn 2016) and electrolyte (Wu et al. 2015) can affect the DSSC performances (Wang et al. 2009).

Metal oxide-based DSSCs focused mainly on tin oxide (Snaith and Ducati 2010), titanium oxide (TiO_2) (Erten, Eren, and İcli 2007; Erten-Ela 2012) and zinc oxide (Beek, Wienk, and Janssen 2004) as the electron acceptor to replace high-cost platinum (Pt) counter electrodes (Erten-Ela and Turkmen 2011; Oh, Yuan, and Branz 2012). The functionality of these materials has been considered not only for their power conversion efficiencies but also for their dye-uptaking capability and durabilities (Erten-Ela et al. 2015). For instance, tin oxide has been studied more than TiO_2 because of its long-term stability, higher carrier mobility and deeper conduction band (Snaith and Ducati 2010); on the other hand, tin oxide showed major limitations in dye-uptaking that decrease its photon-to-electron conversion efficiency (Erten-Ela et al. 2015). Therefore, research on alternative material studies for DSSC fabrication provides fundamental understanding

and new approaches to increase the photon-to-electron conversion efficiency and stability in a low-cost frame.

In this work, we designed new hybrid nanostructured counter electrodes for DSSCs. Inorganic materials of molydenum disulphide (MoS_2) nanotube and tungsten oxide ($W_{18}O_{49}$) nanowire were nanocoated with conducting polymers of poly(3-hexylthiophene) (P3HT) and poly(3,4-ethylene-dioxythiophene) (PEDOT) via solvent-free plasma modification to provide an interpenetrating network for bulk-heterojunction systems. To date, MoS_2 (Wu et al. 2011; Yue et al. 2013; Song et al. 2014) and $W_{18}O_{49}$ (Erten-Ela et al. 2015; Wu et al. 2011; Yang and Ni 2012; Yue et al. 2013; Song et al. 2014) for DSSCs have been minimally studied, despite their easy modification and good catalytic activity. By means of increased surface area of inorganic materials such as MoS_2 nanotube and $W_{18}O_{49}$ nanowire (e.g. electron acceptor), and conducting polymers of P3HT and PEDOT (e.g. electron donor matrix) hybrids can be used to achieve improved donor–acceptor interfacial areas for DSSC that increase photogenerated excitons and high charge/hole/electron mobilities (Bouclé, Ravirajan, and Nelson 2007; Yang and Ni 2012; Song et al. 2014).

Polymer-inorganic bulk-heterojunction systems have been prepared mostly via wet chemical synthesising procedures: (1) a planar bilayer structure where an organic layer is deposited on top of an inorganic semiconductor layer, (2) a simple mixture of polymer and semiconductor nanoparticles and (3) *in situ* polymerisation in the presence of nanomaterials (Bouclé, Ravirajan, and Nelson 2007; Song et al. 2014). These solution-based hybridisation methods have drawbacks in control of the morphology of the materials and random distribution of nanoparticles within the polymer, which result in inadequate electrical contact (Kiristi et al. 2014). Thus, use of the hybrid as an electrode can be hampered by the fact that only the polymer matrix has direct electrical connection to the electrode. Unlike solution-based hybridisation methods, radio frequency (RF, 13.56 MHz) plasma modification provides solvent-free, homogenous and controllable nanocoatings for the materials (Karahancer et al. 2014; Kiristi et al. 2014). The RF-plasma process contains reactive species (positive and negative ions, atoms, neutrals, metastables and free radicals) of the materials, resulting in chemically stable nanocoatings (Denes and Manolache 2004; Lakshmi et al. 2010; Kiristi et al. 2015). Recently, RF-plasma modification processing has been used to coat TiO_2 nanomaterials by polythiophene plasma (Uygun Oksuz et al. 2013) and coating of chitosan powders by hydrazine plasma (Uygun et al. 2011). In these studies, single-step RF-plasma treatment exhibited homogenous nanocoating around the solid particles without molecular degradation (Uygun et al. 2011; Uygun Oksuz et al. 2013; Kiristi et al. 2014).

In this work, MoS_2 nanotube and $W_{18}O_{49}$ nanowire structures were fabricated by a chemical synthesising method and then modified by P3HT and PEDOT RF-plasma method to obtain the hybrid nanostructured materials employed as counter electrodes in DSSCs. Transmission electron microscopy (TEM) surface analysis was conducted to investigate RF-plasma-modified hybrid nanostructures. Chemical compositions of hybrid nanomaterials were studied by energy-dispersive X-ray spectroscopy (EDS) analysis and indicated the plasma hybridisation. Photovoltaic (PV) performance studies showed MoS_2/PEDOT, MoS_2/P3HT, $W_{18}O_{49}$/PEDOT and $W_{18}O_{49}$/P3HT hybrid nanostructures as counter electrode catalysts for low-cost and efficient DSSCs.

2. Experimental section

2.1. MoS_2 nanotube and $W_{18}O_{49}$ nanowire fabrication

$W_{18}O_{49}$ nanowires were synthesised by an iodine transport method (Remškar et al. 2007) using nickel as a growth promoter, WO_3 as a source of tungsten and oxygen and W for reduction of WO_3. The starting material, which consisted of 352.7 mg WO_3 powder (Sigma-Aldrich, 99.99%), 20 mg W (Sigma-Aldrich), 37.5 mg nickel (mechanically cut metal foil) and 562 mg iodine (1–3 mm beads, Sigma-Aldrich, 99.7%), was evacuated in quartz ampoule, sealed and put into a

two-zone furnace. The temperature was increased for 24 h from room temperature to the working conditions. Material was transported from the hot zone (860°C) to the cold zone at (736°C) of the furnace under 6.2°C/cm temperature gradient. Transport reaction was run for 500 h and then cooled down under a 35°/h cooling rate. Transported material of deep violet colour consisted of long nanowires.

MoS$_2$ nanotubes were obtained via sulphurisation of Mo$_6$S$_2$I$_8$ nanowires (Remškar, Viršek, and Mrzel 2009; Ković et al. 2013). Sulphurisation took place at 1173 K in flowing Ar gas containing 2% H$_2$S and 1% H$_2$ and lasted for 3 h. The precursor nanowires were synthesised at 1320 K directly from elements; molybdenum (powder, <150 micron, 99.99%, Sigma-Aldrich), sulphur (flakes, >99.99%, Sigma-Aldrich) and iodine (1–3 mm beads, Sigma-Aldrich, 99.7%), in a molar ratio of 6:2:8.

2.2. RF-plasma modification of MoS$_2$ and W$_{18}$O$_{49}$

Modification of MoS$_2$ and W$_{18}$O$_{49}$ was carried out in a capacitively coupled, RF (13.56 MHz) rotating plasma reactor, separately (Kiristi et al. 2014). To modify nanomaterials, the plasma of the dopant agents of EDOT (98% Aldrich) and 3-hexylthiophene (Aldrich) were created in the rotating plasma chamber, separately. Steady-state plasma coating parameters during 30 min of treatment were: base pressure of 20 mTorr; and RF power of 30 W (CW). Both types of film coatings were carried out without a precursor.

Surface morphologies of plasma-modified hybrid nanomaterials were investigated using a high-resolution HR-TEM Jeol 2010F, field emission model TEM analysis device. Elemental analysis was performed by an EDS method using Philips XL-30 S FEG and Tescan Vega LSU.

The Raman spectra were obtained using a WITec CRM200 Raman system with 1800 and 150 lines/mm grating, respectively, with 532 nm excitation laser. X-ray photoelectron spectroscopy (XPS) signals were measured using a Thermo Scientific K-Alpha XPS system (Thermo Fisher Scientific, UK) equipped with a micro-focused, monochromatic Al Kα X-ray source (1486.6 eV). The direct current electrical conductivity of samples was measured by the standard four-probe method using PCI- DAS6014 for a current source, voltameter and temperature controller.

2.3. DSSCs' fabrication of the hybrid MoS$_2$ and W$_{18}$O$_{49}$

The TiO$_2$ films were employed for the anodes in DSSCs. TiO$_2$-coated fluorine-doped Tin Oxide (FTO) glasses were sintered in ambient atmosphere at 450°C for 30 min. The TiO$_2$ electrodes were sensitised overnight by immersing in a dye solution of Z907 (0.5 mmol dm^{-3}), (*cis-Bis(isothiocyanato)(2,2'-bipyridyl-4,4'-dicarboxylato)(4,4'-di-nonyl-2'-bipyridyl)ruthenium (II)*). MoS$_2$/PEDOT, MoS$_2$/P3HT, W$_{18}$O$_{49}$/PEDOT and W$_{18}$O$_{49}$/P3HT hybrid materials and W$_{18}$O$_{49}$ and MoS$_2$ were used instead of Pt in counter electrodes. The pastes of modified and unmodified MoS$_2$ and W$_{18}$O$_{49}$ materials were prepared using dispermat equipment and materials was coated using Doctor blade technique. And FTO-coated glasses were backed at 250°C in an air furnace. The cell was assembled by separating the electrodes by a 2.5 mm thick plastic spacer and injecting the electrolyte by means of capillary force. The 0.6 mol dm^{-3} N-methyl-N-butyl-imidazolium iodide + 0.1 mol dm^{-3} LiI + 0.05 mol dm^{-3} I$_2$ + 0.5 mol dm^{-3} 4-tert-butylpyridine in acetonitrile as redox electrolyte solution was introduced through pre-drilled holes in the counter electrode. I-V characteristics of DSSCs were performed both in the dark and under illumination. Oriel solar simulator and a Keithley 2400 source meter were used to measure the solar cell performances of cells. The external quantum efficiency (EQE) was measured as a function of incident wavelength from 300 to 800 nm using an EQE system specially designed for DSSCs. A 75 W Xe lamp was used to generate a monochromatic beam. EQE values were collected at a low chopping speed of 4 Hz.
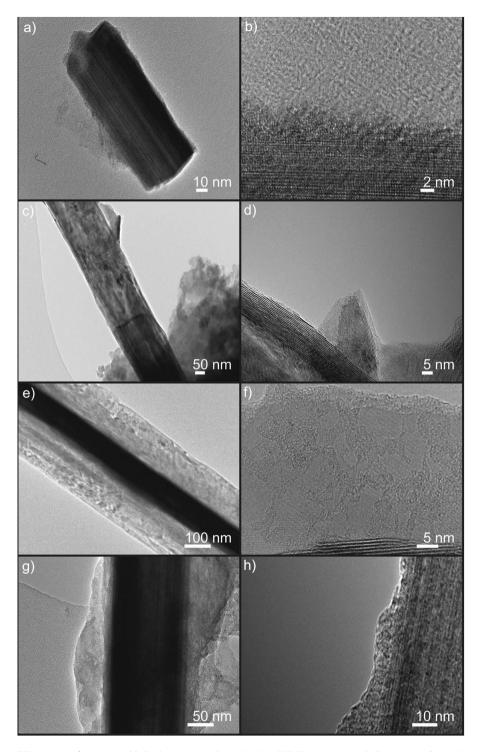
Table 1. Elemental composition of RF-plasma-modified MoS_2 nanotube and $W_{18}O_{49}$ nanowire structures (Mo: molybdenum, W: tungsten, S: sulphur, O: oxygen, C: carbon).

MoS_2 nanotube	Mo (wt%)	S (wt%)	O (wt%)	C (wt%)	$W_{18}O_{49}$ nanowire	W (wt%)	O (wt%)	S (wt%)	C (wt%)
Non-modified MoS_2	25.7	62.2	12	–	Non-modified $W_{18}O_{49}$	26.3	73.7	–	–
MoS_2–PEDOT	3.2	6.6	1.9	88.3	$W_{18}O_{49}$–PEDOT	0.1	5.5	2.8	91.5
MoS_2–P3HT	6.1	13.3	2.5	78	$W_{18}O_{49}$–P3HT	1.5	10.6	7.5	80.3

3. Results and discussion

The atomic composition of the hybrid structures were evaluated by EDS analysis and are presented in Table 1 for RF-plasma-modified MoS_2 nanotube and $W_{18}O_{49}$ nanowire hybrid structures. The total elemental ratio of metal components decreased with the increasing ratio of modifying agents of PEDOT and P3HT in the structure after RF-plasma treatments. A significantly increased amount of carbon contents in the plasma-modified samples indicates the achievement of hybridisation of MoS_2 nanotube and $W_{18}O_{49}$ nanowire materials by plasma polymers (Karahancer et al. 2014; Kiristi et al. 2014, 2015) Sulphur amount in the hybrid structure played a key role in the catalytic activity of the counter electrode of DSSCs (Wu et al. 2011; Yang and Ni 2012; Yue et al. 2013; Song et al. 2014).

TEM images clearly show that the plasma nanocoatings of MoS_2 and $W_{18}O_{49}$ nanostructures have been achieved, and PEDOT and P3HT appeared as a second layer around the polycrystalline structure of nanomaterials after RF-plasma treatments (Figure 1(a–h)). The RF-plasma modification agents (PEDOT and P3HT) are also intercalated between the nanomaterial layers. It is possible that polymer chains condense at the surface steps and cause this unusual contrast (Figure 1(b,d, f)). The HR-TEM images in Figure 1(a–h) reveal that all nanostructures were well covered with conducting polymer layers after RF-plasma polymerisations (Karahancer et al. 2014; Kiristi et al. 2014, 2015). These nanostructured morphologies lead to increased photocurrent generation relative to a bilayer structure with a planar interface ((Bouclé, Ravirajan, and Nelson 2007). Bulk-heterojunction morphology of MoS_2/PEDOT, MoS_2/P3HT, $W_{18}O_{49}$/PEDOT and $W_{18}O_{49}$/P3HT hybrid materials enhance the interfacial area where the photogenerated excitons are dissociated into charge carriers and increase the surface-to-volume ratio for maximum dye loading (Beek, Wienk, and Janssen 2004; Erten-Ela et al. 2015).

The Raman spectra of MoS_2 nanotubes show two typical Raman active vibration modes: an in-plane (E2g) mode located around 384 cm^{-1} and an out-of-plane (A1g) mode which is located at 408 cm^{-1}. These values match the positions obtained in bulk MoS_2 (383 cm^{-1}, 409 cm^{-1}) (Wieting and Verble 1971). The in-plane mode corresponds to the sulphur atoms vibrating in one direction and the molybdenum atoms in the other, while the out-of-plane mode describes vibration of sulphur atoms out-of-plane. In the MoS_2–PEDOT composite, there is no additional Raman active modes in the measured range, while in the MoS_2–P3HT, five additional peaks are present: 287, 337, 668, 826 and 998 cm^{-1}. Besides, the relative intensity of MoS_2 Raman peaks is changed. While in pure MoS_2 nanotubes, and in MoS_2–PEDOT composite, the A_{ig} peak strongly dominates the spectra, it is much suppressed in the MoS_2–P3HT composite. This suppression can indicate a strong interaction between MoS_2 nanotubes and their surroundings, which affects the out-of-plane vibration mode of MoS_2. The presence of other Raman peaks in the MoS_2–P3HT spectrum cannot be explained as completely polymerised P3HT, which has typical Raman modes at 1379.3 cm^{-1} (C-C skeletal stretching) and at 1447.4 cm^{-1} (C=C) symmetric stretching (Obreja et al. 2013). The absence of these two typical modes and the presence of other Raman peaks indicate that the polymerisation was not complete. The additional peaks, 287, 337, 668, 826 and 998 cm^{-1}, can be attributed to MoO_3 (Seguin et al. 1995). The presence of the oxide peaks in the spectrum means that the MoS_2 nanotubes got oxidised either during Raman spectroscopy or during the plasma-assisted polymer coating process.

Figure 1. TEM images of nanocoated hybrid nanomaterials: (a) $W_{18}O_{49}$–PEDOT nanowire (scale bar 10 nm), (b) $W_{18}O_{49}$–PEDOT nanowire (scale bar 2 nm); (c) MoS_2–PEDOT (scale bar 50 nm), (d) MoS_2–PEDOT (scale bar 5 nm); (e) MoS_2–P3HT (scale bar 100 nm); (f) MoS_2–P3HT (scale bar 5 nm); (g) $W_{18}O_{49}$–P3HT (scale bar 50 nm); (h) $W_{18}O_{49}$–P3HT (scale bar 10 nm).

The Raman spectrum of $W_{18}O_{49}$ shows four main peaks in the measured region positioned at 131, 264, 711 and at 807 cm^{-1}. While the first one matches with the value from literature (Guo et al. 2012), the positions of the other peaks slightly differ from the reported values (259, 702 and 803 cm^{-1}). The peaks are attributed to the following vibration modes: 131 cm^{-1} to W–O–W bending modes, 259 cm^{-1} to O–W–O bending modes and 711 and 807 cm^{-1} to W–O stretching modes (Lu et al. 2007). Deviation of our results from the reported ones can be explained with currently unknown peculiarities in the structure of our nanowires, which affect only O–W–O bending modes and W–O stretching modes. In both Raman spectra of the composites, the peak at 264 cm^{-1} is suppressed relatively to other $W_{18}O_{49}$ peaks, the most in the $W_{18}O_{49}$–P3HT composite. This suppression reveals an interaction between the nanowires and the polymers. In both polymer composites, an additional peak appeared: at 890 cm^{-1} in $W_{18}O_{49}$–PEDOT and at 885 cm^{-1} in $W_{18}O_{49}$–P3HT. These peaks are hints about explanation of experimentally obtained IR peak in PEDOT spectra at 892 cm^{-1}, which was attributed to oxyethylene ring deformation vibrations (Tang et al. 2015) (Figures 2 and 3).

XPS was also used to examine the surface composition profiles of MoS_2 and $W_{18}O_{49}$ before and after plasma modification by using PEDOT and P3HT (Figures 4–5).

XPS results show Mo-peak, which is characteristic for Mo^{4+} (229.5 eV) (Tang et al. 2015), which is typical for MoS_2 as seen Figure 4. There is no indication of Mo^{6+} (232.9 eV), which would
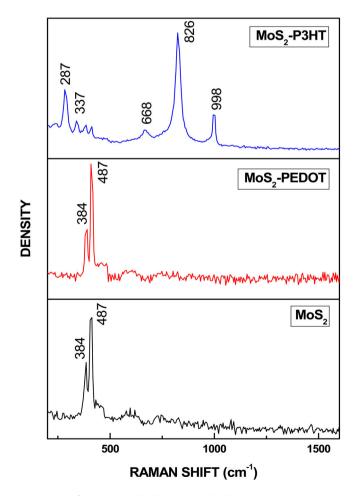

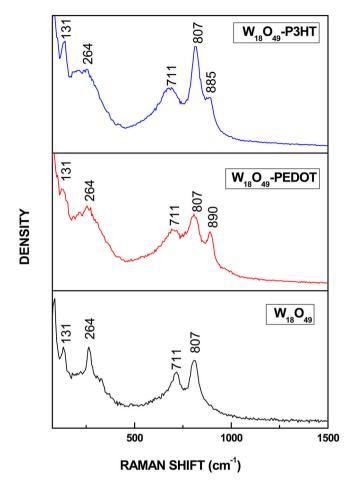Figure 2. Raman spectra comparison of MoS_2, MoS_2/PEDOT and MoS_2/P3HT.

Figure 3. Raman spectra of $W_{18}O_{49}$, $W_{18}O_{49}$/PEDOT and $W_{18}O_{49}$/P3HT.

represent MoO_3. The oxygen peak in MoS_2 (530 eV) can be attributed to metal oxide, that is, Mo-O (MoO_3 or MoO_3-x). In the MoS_2/PEDOT the value (530.95 eV) is larger and indicates the presence of C–O bonds. The largest value (533.61 eV) in the MoS_2–P3HT sample reveals the presence of C=O bonds. A small deviation of the positions of the carbon peaks at 284.8 eV can be explained with a slight charge effect. The S2p peaks for sulphur atoms were obtained at 161.52 and 161.53 eV after P3HT and PEDOT coatings, respectively (Lee et al. 2014).

The XPS results of $W_{18}O_{49}$, $W_{18}O_{49}$/P3HT and $W_{18}O_{49}$/PEDOT are given in Figure 5. In XPS spectrum of $W_{18}O_{49}$, the peak of W4f spectra positioned at 36.08 is assigned to the W in the W–O bond configuration, while a peak position at 530.08 eV is assigned to the oxygen (Li et al. 2014). Position of the energy scale was adjusted to place the main C 1s feature (C–C) at 285.0 eV.

XPS spectra of $W_{18}O_{49}$/P3HT and $W_{18}O_{49}$/PEDOT indicate 162.07 and 161.87 eV peaks corresponding to the C–S signal of thiophene moieties on the surface.

3.1. Photovoltaic performances of DSSCs with different counter electrodes

Photocurrent–voltage (J–V) characteristic curves of solar cells under simulated sunlight irradiation are shown in Figure 6 for MoS_2/PEDOT, MoS_2/P3HT, $W_{18}O_{49}$/PEDOT and $W_{18}O_{49}$/P3HT
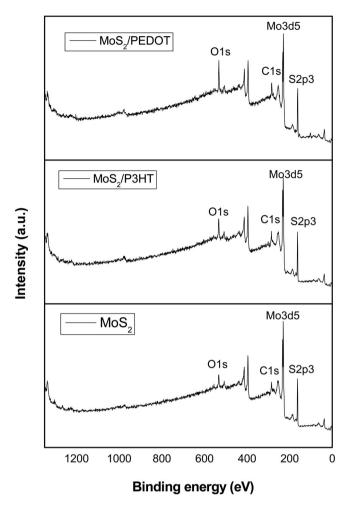
Figure 4. XPS data of MoS_2, MoS_2/PEDOT and MoS_2/P3HT.

hybrid counter electrodes (Scheme 1). As a comparison, the functional properties of the cells fabricated using the same photoanode sensitised by Z907 ruthenium complex dye is shown. The overall conversion efficiencies increase in the range of MoS_2/P3HT > MoS_2/PEDOT > $W_{18}O_{49}$/PEDOT > $W_{18}O_{49}$/P3HT hybrid counter electrodes. Table 2 summarises the PV parameters obtained from J–V curves (Figure 6) of DSSCs with four different counter electrodes measured under the illumination of 100 mW/cm^2. Under the standard global AM 1.5 solar irradiation, a MoS_2/PEDOT-based counter electrode in DSSC gave a short circuit density (J_{sc}) of 7.95 mA cm^{-2}, an open circuit voltage (V_{oc}) of 400 mV and a fill factor of 0.46, corresponding to an overall conversion efficiency of 1.45. In the same condition, MoS_2/P3HT-based counter electrode in DSSC exhibited a short circuit density of 9.49 mA cm^{-2}, V_{oc} of 500 mV and a fill factor of 0.31, corresponding to an overall conversion efficiency of 1.47. Solar cell efficiencies are less when $W_{18}O_{49}$/PEDOT and $W_{18}O_{49}$/P3HT counter electrodes were used in DSSCs. Efficiencies changed from 0.19 to 0.17 for $W_{18}O_{49}$/PEDOT and $W_{18}O_{49}$/P3HT counter electrodes, respectively. These obtained data show that Pt counter electrode performance is still higher in DSSCs (Wu et al. 2011; Song et al. 2014), but results show that these nanostructured morphologies are promising as counter electrodes. Inorganic/organic composites comprised metal oxides or
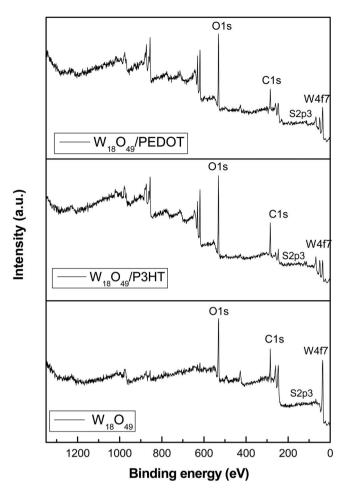
Figure 5. XPS data of $W_{18}O_{49}$, $W_{18}O_{49}$/PEDOT and $W_{18}O_{49}$/P3HT.

metal sulphides and polymer is explored as a promising candidate for the counter electrode in DSSCs. Transition metal sulphides have attracted extensive investigation because of their unique catalytic and electrical characteristics. These results clearly show that MoS_2 nanotubes studied here are better catalysts for tri-iodide reaction than $W_{18}O_{49}$ nanowires. MoS_2 and its nanotube composites have more amorphous surfaces and better conductivities (Table 3) than $W_{18}O_{49}$ and its composite nanowires.

The best results were obtained with MoS_2/P3HT, resulting in a power conversion efficiency almost double in respect to the $W_{18}O_{49}$-based devices, due to a better current density and fill factor, and especially due to a much higher voltage as 200 mV (Table 2). Conductivity measurement confirmed that MoS_2/P3HT composite electrode exhibited better catalytic activity compared to $W_{18}O_{49}$-based composite counter electrodes.

Performance results of the best DSSC were confirmed by EQE measurement. Figure 7 exhibits the EQE of DSSCs. From EQE measurements, the MoS_2/P3HT and MoS_2/PEDOT show higher incident photon to converted electron (IPCE) yields at 456 nm of 55.70% and 49.34%, respectively. It can be concluded that sulphides improved the catalytic activities.

$W_{18}O_{49}$/PEDOT and $W_{18}O_{49}$/P3HT show an IPCE yield at 456 nm of 15.80%. Results show that MoS_2/ PEDOT- and MoS_2/P3HT-coated counter electrodes are very promising materials in DSSCs. The catalytic activities of MoS_2/PEDOT and MoS_2/P3HT hybrid nanotubes in DSSCs are
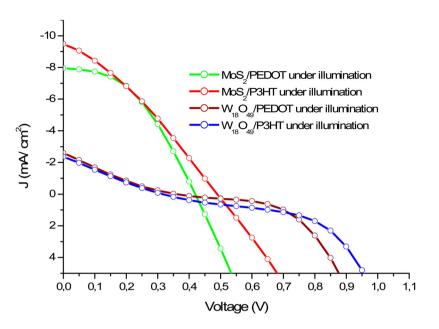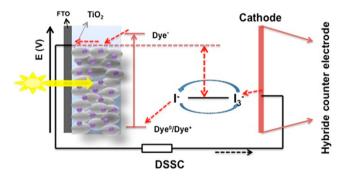
Figure 6. Photocurrent–voltage (*J–V*) characteristic of DSSCs in the dark and under illumination.

Scheme 1. Simplified diagram of DSSC.

higher than $W_{18}O_{49}$/PEDOT and $W_{18}O_{49}$/P3HT nanowires. According to DSSC performances, MoS_2 nanotube materials show better catalytic activities than $W_{18}O_{49}$ nanowire. Moreover, the conversion efficiencies, η (%) of hybrid DSCCs are higher than those of pure nanostructures (Table 2, Figure 6, Figure 8).

Table 2. Photovoltaic performance of RF-plasma-modified counter electrodes in DSSCs (short circuit density: J_{sc} (mA cm^{-2}); open circuit voltage: V_{oc} (mV); fill factor (FF); conversion efficiency: η (%)).

	J_{sc} (mA cm^{-2})	V_{oc} (mV)	FF	η (%)
MoS_2/P3HT	9.49	500	0.31	1.47
MoS_2/PEDOT	7.95	400	0.46	1.45
$W_{18}O_{49}$/PEDOT	2.59	350	0.20	0.19
$W_{18}O_{49}$/P3HT	2.37	300	0.24	0.17
MoS_2	4.81	500	0.16	0.39
$W_{18}O_{49}$	1.91	350	0.14	0.09

Table 3. Four-probe conductivity values of samples.

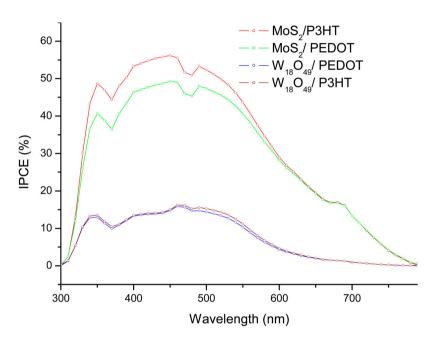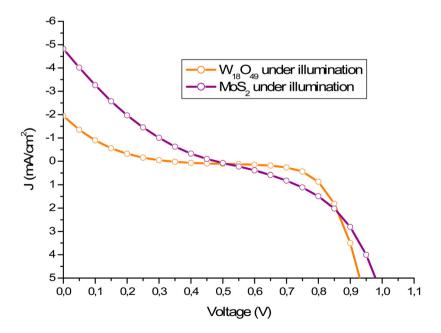| Samples	Conductivity (S/cm)
MoS_2/P3HT	2.5×10^{-3}
MoS_2/PEDOT	1×10^{-3}
$W_{18}O_{49}$/PEDOT	2.5×10^{-4}
$W_{18}O_{49}$/P3HT	1.39×10^{-5}
MoS_2	1.4×10^{-3}
$W_{18}O_{49}$	1×10^{-4}

Figure 7. IPCE curve of DSSCs.

Figure 8. Photocurrent–voltage (J–V) characteristic of DSSCs in the dark and under illumination.

4. Conclusions

The novel inorganic/organic nanocomposites of MoS_2/PEDOT, MoS_2/P3HT, $W_{18}O_{49}$/PEDOT and $W_{18}O_{49}$/P3HT hybrid materials were obtained through solvent-free single-step RF-plasma processing. Employing these hybrid nanostructures as counter electrodes, the DSSCs exhibit PV performance comparable with those using Pt counter electrodes. MoS_2 acts as active sides for the tri-iodide reduction and P3HT improves the electrical performance. These results have confirmed that the novel RF-plasma-modified hybrid nanostructures have potential for the use as low-cost, printable and as Pt-free counter electrode materials. The cathode for DSSCs can be an alternative route towards a cost-effective green energy conversion.

References

Beek, W. J. E., M. M. Wienk, and R. A. J. Janssen. 2004. "Efficient Hybrid Solar Cells From Zinc Oxide Nanoparticles and a Conjugated Polymer." *Advanced Materials* 16 (12): 1009–1013. doi:10.1002/adma.200306659.

Bouclé, J., P. Ravirajan, and J. Nelson. 2007. "Hybrid Polymer–metal Oxide Thin Films for Photovoltaic Applications." *Journal of Materials Chemistry* 17: 3141–3153. doi:10.1039/B706547G.

Briscoe, Joe, and Steve Dunn. 2016. "The Future of Using Earth-Abundant Elements in Counter Electrodes for Dye-Sensitized Solar Cells." *Advanced Materials* 28 (20): 3802–3813. doi:10.1002/adma.201504085.

Denes, F. S., and S. Manolache. 2004. "Macromolecular Plasma-chemistry: An Emerging Field of Polymer Science." *Progress in Polymer Science* 29 (8): 815–885. doi:10.1016/j.progpolymsci.2004.05.001.

Erten, S., E. Eren, and S. İcli. 2007. "Dye Sensitized Solar Cell Based on 1,8-Naphthalene Benzimidazole Comprising Carboxyl Group." *The European Physical Journal Applied Physics* 38: 227–230. doi:10.1051/epjap:2007086.

Erten-Ela, S. 2012. "Photovoltaic Effect of Nanostructured TiO_2 Layers in Dye Sensitized Solar Cells." *Journal of Optoelectronics and Advanced Materials* 14 (9-10): 758–762. Accessed May 1 2016. http://pubs.rsc.org/en/content/articlehtml/2013/ee/c3ee24453a.

Erten-Ela, S., and G. Turkmen. 2011. "Perylene Imide Dyes for Solid-State Dye-sensitized Solar Cells: Spectroscopy, Energy Levels and Photovoltaic Performance." *Renewable Energy* 36 (6): 1821–1825. doi:10.1016/j.renene.2010.11.025.

Erten-Ela, S., C. Villegas, J. L. Delgado, and N. Martin. 2015. "Pyrrolidino [60] and [70]Fullerene Homo- and Heterodimers as Electron Acceptors for OPV." *New Journal of Chemistry* 39 (2): 1477–1482. doi:10.1039/C4NJ01709A.

Guo, C., S. Yin, Q. Dong, and T. Sato. 2012. "The Near Infrared Absorption Properties of $W_{18}O_{49}$." *RSC Advances* 2: 5041–5043. doi:10.1039/C2RA01366E.

Huang, An-Ni, Wen-Chu Pien, and Hsiu-Po Kuo. 2014. "Preparation of the Working Electrode of Dye-sensitized Solar Cells Using Screen Printing with Alkyd Resins." *Energy Procedia* 61: 1528–1531. doi:10.1016/j.egypro.2014.12.162.

Karahancer, S. S., M. Kiristi, S. Terzi, M. Saltan, A. Uygun Oksuz, and L. Oksuz. 2014. "Performance Evaluation of Nano-modified Asphalt Concrete." *Construction and Building Materials* 71: 283–288. doi:10.1016/j.conbuildmat.2014.08.072.

Kiristi, M., F. Bozduman, A. Uygun Oksuz, A. Hala, and L. Oksuz 2015. "A Comparison Study of Microwave and Radio Frequency Plasma Polymerized PEDOT Thin Films." *Journal of Macromolecular Science, Part A* 52 (2): 124–129. doi:10.1080/10601325.2015.980762.

Kiristi, M., F. Bozduman, A. Uygun Oksuz, L. Oksuz, and A. Hala. 2014. "Solid State Electrochromic Devices of Plasma Modified WO_3 Hybrids." *Industrial & Engineering Chemistry Research* 53 (41): 15917–15922. doi:10.1021/ie5025613.

Ković, Adrej, Damjan Vengust, Mojca Vilfan, and Aleš Mrzel. 2013. "Controlled Self-decoration of $Mo_6S_yI_z$ (8.2 ≤ y + z ≤ 10) Nanowires and Their Transformation to MoS_2 Nanotubes with Gold Nanoparticles." *Journal of Nanoparticle Research* 15:1791. doi:10.1007/s11051-013-1791-2.

Lakshmi, G. B. V. S., A. Dhillon, D. K. Avasthi, A. M. Siddiqui, and M. Zulfequar. 2010. "Synthesis and Characterization of Thin Films of Poly(3-Methyl Thiophene) by rf-Plasma Polymerization." *Materials Letters* 64 (15): 1672–1673. doi:10.1016/j.matlet.2010.04.055.

Lee, S. H., H. Park, S. Kim, W. Son, I. W. Cheong, and J. H. Kim. 2014. "Transparent and Flexible Organic Semiconductor Nanofilms with Enhanced Thermoelectric Efficiency." *Journal of Materials Chemistry A* 2: 7288–7294. doi:10.1039/C4TA00700J.

Li, X., S. Yang, J. Sun, P. He, X. Xu, and G. Ding. 2014. "Tungsten Oxide Nanowire-Reduced Graphene Oxide Aerogel for High-efficiency Visible Light Photocatalysis." *Carbon* 78: 38–48. doi:10.1016/j.carbon.2014.06.034.

Lu, D. Y., J. Chen, Z. Zhou, S. Z. Deng, N. S. Xu, and J. B. Xu. 2007. "Raman Spectroscopic Study of Oxidation and Phase Transition in $W_{18}O_{49}$ Nanowires." *Journal of Raman Spectroscopy* 38 (2): 176–180. doi:10.1002/jrs.1620.

Obreja, A. C., D. Cristea, R. Gavrila, V. Schiopu, A. Dinescu, M. Danila, and F. Comanescu. 2013. "Isocyanate Functionalized Graphene/P3HT Based Nanocomposites." *Applied Surface Science* 276: 458–467. doi:10.1016/j.apsusc.2013.03.117.

Oh, J., H. C. Yuan, and H. M. Branz. 2012. "An 18.2%-Efficient Black-Silicon Solar Cell Achieved Through Control of Carrier Recombination in Nanostructures." *Nature Nanotechnology* 7: 743–748. doi:10.1038/nnano.2012.166.

O'Regan, Brian, and Michael Grätzel. 1991. "A Low-cost, High-efficiency Solar Cell Based on Dye-Sensitized Colloidal TiO_2 Films." *Nature* 353 (6346): 737–740. doi:10.1038/353737a0.

Remškar, M., J. Kovač, M. Viršek, M. Mrak, A. Jesih, and A. Seabaugh. 2007. "W_5O_{14} Nanowires." *Advanced Functional Materials* 17: 1974–1978. doi:10.1002/adfm.200601150.

Remškar, M., M. Viršek, and A. Mrzel. 2009. "The MoS_2 Nanotube Hybrids." *Applied Physics Letters* 95: 133122. doi:10.1063/1.3240892.

Seguin, L., M. Figlarz, R. Cavagnat, and J. C. Lassegues. 1995. "Infrared and Raman Spectra of MoO_3 Molybdenum Trioxides and $MoO_3.xH_2O$ Molybdenum Trioxide Hydrates." *Spectrochimica Acta Part A: Molecular and Biomolecular Spectroscopy* 51 (8): 1323–1344. doi:10.1016/0584-8539(94)00247-9.

Snaith, Henry J., and Caterina Ducati. 2010. "SnO_2-Based Dye-sensitized Hybrid Solar Cells Exhibiting Near Unity Absorbed Photon-to-electron Conversion Efficiency." *Nano Letters* 10 (4): 1259–1265. doi:10.1021/nl903809r.

Song, D., M. Li, Y. Jiang, Z. Chen, F. Bai, Y. Li, and B. Jiang. 2014. "Facile Fabrication of MoS_2/PEDOT–PSS Composites as Low-Cost and Efficient Counter Electrodes for Dye-sensitized Solar Cells." *Journal of Photochemistry and Photobiology A: Chemistry* 279: 47–51. doi:10.1016/j.jphotochem.2014.01.009.

Susanti, Diah, Maula Nafi, Hariyati Purwaningsih, Rindang Fajarin, and George Endri Kusuma. 2014. "The Preparation of Dye Sensitized Solar Cell (DSSC) From TiO_2 and Tamarillo Extract." *Procedia Chemistry* 9: 3–10. doi:10.1016/j.proche.2014.05.002.

Tang, H., J. Wang, H. Yin, H. Zhao, D. Wang, and Z. Tang. 2015. " Growth of Polypyrrole Ultrathin Films on MoS_2 Monolayers as High-Performance Supercapacitor Electrodes." *Advanced Materials* 27 (6): 1117–1123. doi:10.1002/adma.201404622.

Thomas, Sara, T. G. Deepak, G. S. Anjusree, T. A. Arun, V. Nair Shantikumar, and Nair A. Sreekumaran. 2014. "A Review on Counter Electrode Materials in Dye-sensitized Solar Cells." *Journal of Materials Chemistry A* 2 (13): 4474–4490. doi:10.1039/C3TA13374E.

Uygun, A., M. Kiristi, L. Oksuz, S. Manolache, and S. Ulusoy. 2011. "RF Hydrazine Plasma Modification of Chitosan for Antibacterial Activity and Nanofiber Applications." *Carbohydrate Research* 346 (2): 259–265. doi:10.1016/j.carres.2010.11.020.

Uygun Oksuz, A., S. Manolache, L. Oksuz, and N. Hershkowitz. 2013. "Plasma Nanocoating of Thiophene Onto TiO_2 Nanoparticles." *Industrial & Engineering Chemistry Research* 52 (19): 6610–6616. doi:10.1021/ie303176j.

Wang, Mingkui, Alina M. Anghel, Benoit Marsan, Ngoc-Le Cevey Ha, Nuttapol Pootrakulchote, Shaik M. Zakeeruddin, and Michael Gratzel. 2009. "CoS Supersedes Pt as Efficient Electrocatalyst for Triiodide Reduction in Dye-Sensitized Solar Cells." *Journal of the American Chemical Society* 131 (44): 15976–15977. doi:10.1021/ja905907y.

Wieting, T. J., and J. L. Verble. 1971. "Infrared and Raman Studies of Long-wavelength Optical Phonons in Hexagonal MoS_2." *Physical Review B* 3 (12): 4286–4292.

Wu, Jihuai, Zhang Lan, Jianming Lin, Miaoliang Huang, Yunfang Huang, Leqing Fan, and Genggeng Luo. 2015. "Electrolytes in Dye-sensitized Solar Cells." *Chemical Reviews* 115 (5): 2136–2173. doi:10.1021/cr400675m.

Wu, M., Y. Wang, X. Lin, N. Yu, L. Wang, L. Wang, A. Hagfeldt, and T. Ma. 2011. "Economical and Effective Sulfide Catalysts for Dye-sensitized Solar Cells as Counter Electrodes." *Physical Chemistry Chemical Physics* 13: 19298–19301. doi:10.1039/c1cp22819f.

Yang, Z., and X. Ni. 2012. "Photovoltaic Hybrid Films with Polythiophene Growing on Monoclinic WO₃ Semiconductor Substrates." *Langmuir* 28 (10): 4829–4834. doi:10.1021/la204990d.

Yue, G., Wu, J., Xiao, Y., Huang, M., Lina, J., and Lin, J.-Y. 2013. "High Performance Platinum-free Counter Electrode of Molybdenum Sulfide–Carbon Used in dye-Sensitized Solar Cells." *Journal of Materials Chemistry A* 1: 1495–1501. doi:10.1039/C2TA00860B.

Zhang, Shufang, Xudong Yang, Youhei Numata, and Liyuan Han. 2013. "Highly Efficient Dye-sensitized Solar Cells: Progress and Future Challenges." *Energy & Environmental Science* 6 (5): 1443–1464. doi:10.1039/C3EE24453A.